Journal of Catalysis **196,** 352–361 (2000)
doi:10.1006/jcat.2000.3038, available online at http://www.idealibrary.com on IDEAL®

Characterization of Ruthenium-Exchanged Zeolites (Beta, Y, and ZSM-5) by EPR Spectroscopy

Patrick J. Carl and Sarah C. Larsen[1]

Department of Chemistry, University of Iowa, Iowa City, Iowa 52242

Received May 5, 2000; revised August 7, 2000; accepted August 7, 2000

Ruthenium-exchanged zeolites, Ru–Beta, Ru–Y, and Ru–ZSM-5, are active catalysts for the decomposition of nitrous oxide, N_2O. $[Ru(NH_3)_6]^{3+}$ was exchanged into zeolites Y, Beta, and ZSM-5. The resulting ruthenium-exchanged zeolites were characterized by electron paramagnetic resonance (EPR) spectroscopy and were tested for N_2O decomposition activity. The decomposition of the $[Ru(NH_3)_6]^{3+}$ complex in the zeolites during pretreatment in helium at elevated temperatures was monitored using EPR spectroscopy. Ru–Beta and Ru–Y exhibited similar EPR spectra that were interpreted in terms of loss of amine ligands, formation of aquo and hydroxyl ruthenium complexes, and eventual loss of all ligands with binding to zeolitic oxygen. The EPR spectra of Ru–ZSM-5 exhibited some similar spectral features with the exception of the initial $[Ru(NH_3)_6]^{3+}$ complex. The presence of a specific ruthenium species observed by EPR was correlated with the catalytic activity of Ru–Y.

I. INTRODUCTION

Ruthenium-exchanged zeolites are effective heterogeneous catalysts for several different reactions. Ruthenium-exchanged zeolites are active catalysts for the water–gas shift reaction (1), the carbon monoxide–hydrogen methanation reaction (2), and more recently, the decomposition of nitrous oxide (3, 4). There have been a number of studies evaluating the catalytic activity of various ruthenium-exchanged zeolites for nitrous oxide decomposition (3–5). Li and Armor reported that ruthenium and rhodium-exchanged zeolites were the most active transition-metal-exchanged zeolites for N_2O decomposition (3). Chang *et al.* studied nitrous oxide decomposition over ruthenium-exchanged ZSM-5 and USY (4, 5). Using temperature-programmed reduction (TPR) and temperature-programmed oxidation (TPO) experiments, Chang *et al.* concluded that the active form of ruthenium is not ruthenium metal, but rather ionic ruthenium (4).

Ruthenium (Ru^{3+}, d^5) is typically exchanged into the parent zeolite as an amine complex, $[Ru(NH_3)_6]^{3+}$, or an aquo complex, $[Ru(H_2O)_6]^{3+}$. The high-spin and low-spin states of Ru^{3+} are paramagnetic, which makes them amenable to detection by electron paramagnetic resonance (EPR) spectroscopy. The ruthenium-exchanged zeolite is typically pretreated at elevated temperatures in oxygen or helium to produce the active form of the catalyst. The decomposition of the exchanged Ru^{3+} complex during pretreatment can be monitored using EPR spectroscopy to characterize paramagnetic intermediates and to determine the ruthenium species that may be responsible for the catalytic activity. Previously, several groups have used EPR spectroscopy to study the Ru^{3+} species formed from the decomposition of $[Ru(NH_3)_6]^{3+}$ exchanged into NaY and MX (M = H, Na, Ca, and Li) (6–9). After pretreatment of Ru–X and Ru–Y under vacuum at different temperatures, the EPR signals obtained were assigned to various Ru species (6–8). Based on small molecule (CO, O_2, NO, and H_2O) adsorption studies, the probable location of various Ru species in X- and Y-type zeolites was determined (6–8). No EPR studies of ruthenium-exchanged Beta and ZSM-5 have been previously reported.

The ruthenium complexes formed in ruthenium-exchanged zeolites are influenced by the zeolite structure. Both the topology and Si/Al ratio of the zeolite affect the electronic environment of the exchanged ruthenium ions. In this study, the decomposition of the $[Ru(NH_3)_6]^{3+}$ complex in three different zeolites, ZSM-5, Beta, and Y, was monitored using EPR spectroscopy. The zeolites, ZSM-5, Beta, and Y, have different Si/Al ratios and different channel networks that may lead to different electronic environments for ruthenium ions.

In this paper, the ruthenium-exchanged zeolites, Ru–Beta, Ru–Y, and Ru–ZSM-5, were characterized using EPR spectroscopy. The paramagnetic species formed during the pretreatment of ruthenium-exchanged zeolites were monitored using EPR spectroscopy. Comparison of the EPR spectra of Ru–Beta and Ru–Y indicated similar Ru^{3+} complexes were formed in these two zeolites after pretreatment in helium at elevated temperatures. Ru–ZSM-5 exhibited relatively weak EPR signals until pretreatment temperatures greater than 473 K were reached. The

[1] To whom correspondence should be addressed. Fax: 319-335-1279. E-mail: sarah-larsen@uiowa.edu.

0021-9517/00 $35.00

ruthenium-exchanged zeolites were also evaluated for N_2O decomposition activity. The implications of the EPR results for catalytic activity will be discussed.

II. EXPERIMENTAL

A. Sample Preparation

Ruthenium-exchanged zeolites, Beta(NH_4^+–Beta, Zeolyst Inc.), ZSM-5 (NaZSM-5, Zeolyst Inc.), and Y (Na form, in-house synthesis (10)) were prepared using dilute solutions of $[Ru(NH_3)_6Cl_3]$ (Strem Chemicals, 99%). The parent zeolite (2.0 g) was added to 100 ml of aqueous $[Ru(NH_3)_6Cl_3]$ solution (0.01 M ruthenium(III) for Beta and Y and 0.005 M ruthenium(III) for ZSM-5) and stirred for 24 h at room temperature. The exchanged zeolite samples were then filtered and washed with 1.0 L of deionized water and dried overnight in an oven at 363 K. Exchanged samples were characterized by X-ray powder diffraction (Siemans D5000) and ICP-AES (inductively coupled plasma atomic emission spectroscopy) for elemental analysis. Diffraction patterns agreed well with standard diffraction patterns for zeolites Beta, ZSM-5, and Y. No peaks in the diffraction patterns indicated the presence of ruthenium oxides in the samples. All of the samples were analyzed using ICP-AES (Perkin–Elmer Plasma 400) to determine the Si/Al ratios and the ruthenium loading of the samples. The elemental analysis results are reported in Table 1. Samples that have not been pretreated are referred to as "fresh" samples. Experiments were performed on the ruthenium-exchanged zeolites within a week of preparation to avoid the possibility of degradation of the sample due to prolonged atmospheric exposure. Ruthenium loadings were kept low to minimize both polynuclear complex formation and formation of ruthenium oxide species.

B. EPR Measurements

The experimental system was configured so that *in situ* EPR experiments could be coupled with catalytic activity measurements (11). The system consists of a Bruker EMX61 EPR (electron paramagnetic resonance) spectrometer, a gas flow control system, and a Varian 3400CX GC (gas chromatograph) equipped with a TCD (thermal conductivity detector), an FID (flame ionization detector), and a gas sampling valve (11). The ruthenium-exchanged zeolite sample was placed in an EPR-grade quartz flow tube (i.d. = 1.5 mm) and was held in place by a quartz wool plug. Tylan FC-260 mass flow controllers were used to control the flow of reactant (N_2O in Helium) and pretreatment (Helium) gases through the flow cell. Hydro-Purge water filters (Alltech) were used to remove water from the gases. Product gases were analyzed using GC by injection of a gas sample (0.25 ml) onto a 10-ft, 5-Å molecular sieve column heated to 308 K with the TCD heated to 473 K. The detector was calibrated with 1.01% Nitrogen Primary Standard (Air Products).

For *in situ* EPR experiments, sample pretreatment involved heating approximately 20 mg of the sample under flowing helium (100 ccm) to various temperatures in the range of 373–673 K and holding at the desired temperature for 30 min. Samples were cooled in the EPR cavity to 120 K for data acquisition after heating to each pretreatment temperature. EPR spectra were acquired using a Bruker EMX61 equipped with a PC for spectrometer control and data acquisition. A Bruker ER4111 Variable Temperature Unit with a temperature range of 110–673 K was used to heat and cool the sample. Typical EPR spectral parameters were X-band frequency = 9.43 GHz, modulation amplitude = 10.0 G, and modulation frequency = 100.0 kHz. The magnetic field and microwave frequency were measured using a Hall probe and a frequency counter, respectively.

C. Catalytic Activity Measurements

For catalytic activity measurements, the sample pretreatment involved heating approximately 30 mg of the sample in 100 ccm of helium at 373 K for 1 h followed by heating at 773 K for 1 h. Helium UPC (99.999%, Air Products) and Nitrous Oxide Primary Standard (3.99% balanced with helium, Matheson) were used in these studies. After pretreatment, the Ru-exchanged zeolite was exposed to 3300 ppm nitrous oxide in approximately 50 ccm total flow and the conversion to N_2 at various temperatures under steady-state reaction conditions was measured by GC as described above. The space velocity varied for each experiment but was on the order of 100,000 ml h^{-1} g^{-1}. Two different space velocities were examined for Ru–Beta and the same conversions of N_2O to N_2 were obtained for both.

TABLE 1

Elemental Analysis Results

Sample	Si : Al	Ru : Al	wt% Ru
Ru–Beta	18	0.035	0.29
Ru–ZSM-5	21	0.024	0.20
Ru–Y	2	0.022	0.78

III. RESULTS

In this study, ruthenium was exchanged into the zeolites as $[Ru(NH_3)_6]^{3+}$. Ru^{3+} in $[Ru(NH_3)_6]^{3+}$ is in a low-spin, d^5 electronic configuration and has octahedral symmetry. In the absence of metal–ligand hyperfine interactions, the spin Hamiltonian for an $S = 1/2$, low-spin, d^5 system can be

written as follows:

$$H = g_x \beta H_x S_x + g_y \beta H_y S_y + g_z \beta H_z S_z.$$

Based on this orthorhombic spin Hamiltonian, the observed EPR spectrum of a low-spin, d^5 complex should have three resonances at g_x and g_y and g_z (12). For the axial case, $g_x = g_y = g_\perp$ and $g_z = g_\parallel$ and the spin Hamiltonian reduces to the following equation:

$$H = g_\parallel \beta H_z S_z + g_\perp \beta (H_x S_x + H_y S_y).$$

Based on the spin Hamiltonian above for the axial system, the observed EPR spectrum should have two resonances at $g_\parallel$ and $g_\perp$ (12). Typically, the most intense feature for the axial system is observed at a magnetic field corresponding to $g_\perp$. Ru^{3+} in an octahedral coordination is characterized by a low-lying excited state that produces a short spin-lattice relaxation time (T_1) (9). Since the linewidth is inversely proportional to T_1, a broad EPR line is expected if the spin-lattice relaxation time is very short. Usually, the EPR spectra are recorded at low temperature because T_1 will be longer, resulting in decreased spectral broadening.

During standard pretreatment of the ruthenium-exchanged zeolites, the amine ligands are removed from the complex and may decompose, forming molecular hydrogen and nitrogen according to reaction [1] below:

$$2NH_3 \rightarrow N_2 + 3H_2. \qquad [1]$$

The molecular hydrogen produced during pretreatment of the zeolites can potentially reduce the Ru^{3+} to Ru^{2+}, Ru^{1+}, or Ru^0. Once the $[Ru(NH_3)_6]^{3+}$ complex loses the amine ligands, the ruthenium ions may complex with water, hydroxide ions, or oxygen from the zeolite framework. Various ruthenium species in zeolites X and Y have been observed in prior EPR studies (7–9, 13) and are summarized in Table 2 for comparison with the data presented in this paper.

In this study, the g values for the different ruthenium species were obtained from the EPR spectra. For EPR spectra that contained overlapping spectral features, subtraction of EPR spectra obtained at different temperatures was used to separate spectral components of overlapping signals. The spectral simulation program (Bruker-Simfonia version 1.25) was used to show that the EPR assignments were consistent with the experimental data.

TABLE 2

Previous EPR Assignments for Ru-Exchanged Zeolites

Zeolite	Assigned species	g_1 ($g_\perp$)	g_2 ($g_\parallel$)	g_3	Reference
Ru–HX	$[Ru(NH_3)_6]^{3+}$	2.10	1.74		(7, 8)
Ru–NaY	$[Ru(NH_3)_6]^{3+}$	2.18	1.76		(9)
Ru–HX	$[Ru(NH_3)_5OH]^{2+}$	2.58	2.24	1.71	(8)
Ru–NaY	$[Ru(NH_3)_5OH]^{2+}$	2.68	2.24	1.75	(9)
Ru–HX	$[Ru(H_2O)_nO_{zeo}]^{3+}$	2.08	2.00	1.95	(8)
Ru–Y	$[Ru(H_2O)_5OH]^{2+}$	2.37	1.72		(13)
Ru–HX	Lattice-bound Ru^{3+}	2.17	2.08	1.94	(8)
Ru–HX	$Ru^{4+}O_2^-$	2.029	2.029	2.006	(8)

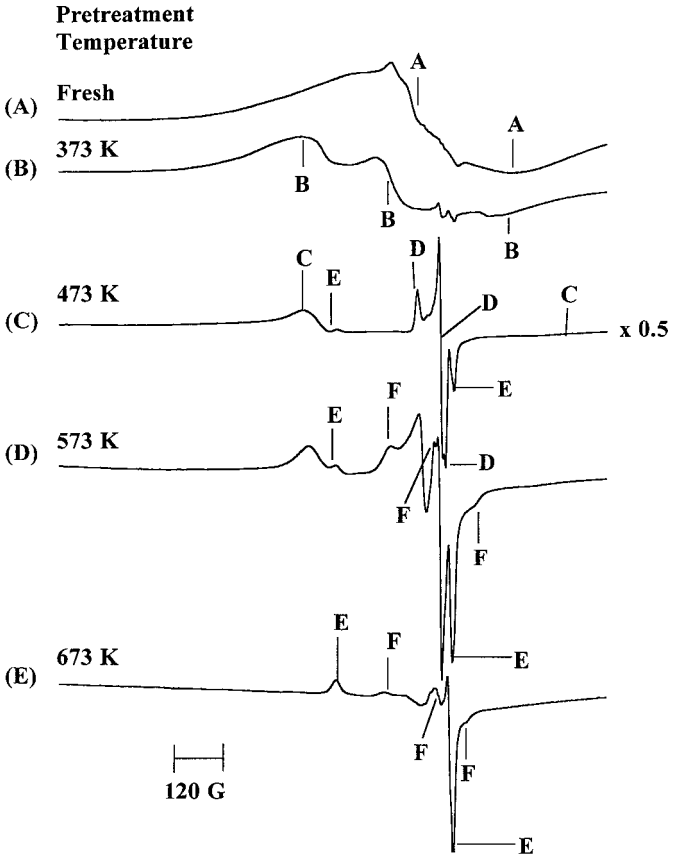

FIG. 1. EPR spectra of Ru–Beta following pretreatment in helium at the indicated temperatures. EPR spectra were acquired at 120 K after sequential heating for 30 min: (A) fresh, (B) 373 K, (C) 473 K, (D) 573 K, and (E) 673 K.

An EPR signal is observed at $g \sim 4.3$ in many of the EPR spectra and is assigned to high-spin Fe^{3+} impurities in the zeolite. The $g \sim 4.3$ signal is observed in EPR spectra of the parent zeolites as well as in the EPR spectra of the ruthenium-exchanged zeolites.

EPR Spectra of Ru–Beta

The color of the Ru–Beta sample changed during the pretreatment procedure. The fresh Ru–Beta sample was white and did not change color during prolonged exposure to air at room temperature. After the standard pretreatment in helium at elevated temperatures, the color of the sample changed to light brown, and after pretreatment followed by exposure to air for several days, the sample color changed to green-gray.

EPR spectra acquired at 120 K of fresh Ru–Beta and Ru–Beta after pretreatment in helium at elevated temperatures (373, 473, 573, and 673 K) are presented in Fig. 1.

TABLE 3

***g* Values and Spectral Assignments for the EPR Spectra of Ru–Beta, Ru–Y, and Ru–ZSM-5 in Figs. 1–3**

Sample	Species	g_1 ($g_\perp$)	g_2 ($g_\parallel$)	g_3	Signal assignment
Ru–Beta (fresh)	A	2.11	1.72		$[Ru(NH_3)_6]^{3+}$
Ru–Beta (373 K)	B	2.56	2.20	1.81	$[Ru(NH_3)_5(OH)]^{2+}$
Ru–Beta (473 K)	C	2.55	1.62		$[Ru(H_2O)_5(OH)]^{2+}$
	D	2.09	1.99	1.98	$[Ru^{3+}(H_2O)_{n-m}(O_{zeo})_m^{-k}]^{3-k}$
	E	1.95	2.42		$[Ru^{3+}(O_{zeo})_m^{-k}]^{3-k}$
Ru–Beta (573 K)	F	2.20	2.02	1.87	$[Ru^{3+}(O_{zeo})_m^{-k}]^{3-k}$
Ru–Y (fresh)	A*	2.00	1.73		$[Ru(NH_3)_6]^{3+}$
Ru–Y (373 K)	B*	2.59	2.22	1.75	$[Ru(NH_3)_5(OH)]^{2+}$
Ru–Y (473 K)	C*	2.47	1.75		$[Ru(H_2O)_5(OH)]^{2+}$
	D*	2.07	2.00		$[Ru^{3+}(H_2O)_{n-m}(O_{zeo})_m^{-k}]^{3-k}$
	E*	1.94	2.41		$[Ru^{3+}(O_{zeo})_m^{-k}]^{3-k}$
	F*	2.21	2.03	1.90	$[Ru^{3+}(O_{zeo})_m^{-k}]^{3-k}$
Ru–Y (673 K)	G	2.69	1.76		$[Ru^{3+}(O_{zeo})_m^{-k}]^{3-k}$
Ru–ZSM-5 (573 K)	D**	2.06	2.01		$[Ru^{3+}(H_2O)_{n-m}(O_{zeo})_m^{-k}]^{3-k}$
	E**	1.95	2.41		$[Ru^{3+}(O_{zeo})_m^{-k}]^{3-k}$

All spectra were recorded at 120 K after heating Ru–Beta to the indicated temperatures for 30 min. The EPR parameters and assignments for these experimental spectra are given in Table 3 and the EPR results from previous studies of Ru–X and Ru–Y are given in Table 2. The letters in Fig. 1 represent the positions of the *g* values for each ruthenium species and correspond to the assignments of the spectral features that are listed in Table 3. The EPR spectrum of fresh Ru–Beta obtained at 120 K exhibits two overlapping signals. No EPR signals were observed at room temperature. The dominant signal (species A) is broad and has EPR parameters, $g_\perp = 2.11$ and $g_\parallel = 1.72$, which are qualitatively similar to those obtained for $[Ru(NH_3)_6]^{3+}$ exchanged into zeolites Ru–HX ($g_\perp = 2.10$, $g_\parallel = 1.74$) (7, 8) and Ru–NaY ($g_\perp = 2.18$, $g_\parallel = 1.76$) (9). Species A, based on previous results for ruthenium-exchanged HX and NaY and from crystal field considerations, is assigned to $[Ru(NH_3)_6]^{3+}$. Ru^{3+} in octahedral symmetry has a low-spin configuration and a low-lying excited state, which produces a small value for the spin-lattice relaxation time (9). The short relaxation time causes a broadening of the line at room temperature. Acquiring spectra at lower temperatures increases the relaxation time so that spectral resolution may be improved. Another signal is also present in the EPR spectrum of fresh Ru–Beta and exhibits a rhombic powder pattern, $g_1 \neq g_2 \neq g_3$. The identity of the second signal was not determined due to the overlap of the spectral features with the broad $[Ru(NH_3)_6]^{3+}$ signal.

After the sample was heated to 373 K (Fig. 1B), the previous EPR signal was replaced by a rhombic signal (species B) that is observable at room temperature, indicating an increase in the spin-lattice relaxation time for this species as compared to species A in the fresh sample. The EPR parameters for species B on Ru–Beta ($g_1 = 2.56$, $g_2 = 2.20$, $g_3 = 1.81$) are similar to those previously assigned to $[Ru(NH_3)_5OH]^{2+}$ in zeolites Ru–NaY ($g_1 = 2.68$, $g_2 = 2.24$, $g_3 = 1.75$) (9) and Ru–HX ($g_1 = 2.58$, $g_2 = 2.24$, $g_3 = 1.71$) (8). This species is most likely formed from the reaction of the $[Ru(NH_3)_6]^{3+}$ complex and adsorbed water to produce $[Ru(NH_3)_5OH]^{2+}$ and NH_4^+.

$$[Ru(NH_3)_6]^{3+} + H_2O \rightarrow [Ru(NH_3)_5OH]^{2+} + NH_4^+. \quad [2]$$

The small variations in g_1 and g_3 when comparing the EPR parameters for species B in Ru–Beta versus previous EPR results for Ru–X and Ru–Y can be attributed to differences in the local environment of the Ru complex. Zeolite Beta has a considerably smaller channel size (5.5×5.5 Å and 7.6×6.4 Å) than the diameter of the alpha cage in zeolites X or Y (~12 Å), which could lead to changes in the local electronic environment and therefore in the *g* values of the ruthenium complex.

As shown in Fig. 1C, the EPR signal changes dramatically after pretreatment of Ru–Beta at 473 K in helium. This change in EPR signal can be attributed to the decomposition of $[Ru(NH_3)_5OH]^{2+}$ and to the formation of new ruthenium species. A sharp, rhombic signal and two features in the low-field region replace the broad rhombic signal due to species B. Three ruthenium species are assigned in the EPR spectrum in Fig. 1C: species C ($g_\perp = 2.55$ and $g_\parallel = 1.62$), species D ($g_1 = 2.09$, $g_2 = 2.00$, $g_3 = 1.98$) and species E ($g_\perp = 1.95$, $g_\parallel = 2.42$). These species were assigned by comparing the EPR spectra in Figs. 1C–1E and by spectral simulation. Further reaction of the amine ligands with adsorbed water is presumed to generate species C, D, and E according to the following reactions:

$$[Ru(NH_3)_5OH]^{2+} + nH_2O \rightarrow [Ru(NH_3)_{5-n}(H_2O)_nOH]^{2+} + nNH_3 \quad [3]$$

$$[Ru(H_2O)_n]^{3+} + mO_{zeo} \rightarrow \left[Ru^{3+}(H_2O)_{n-m}(O_{zeo})_m^{-k}\right]^{3-k} + (n-m)H_2O. \quad [4]$$

The signal for species C is similar in shape and g values to that previously assigned to $[Ru(H_2O)_5OH]^{2+}$ in Ru–Y ($g_\perp = 2.37$, $g_\parallel = 1.72$) (13). Species D has EPR parameters similar to those obtained for Ru–HX ($g_1 = 2.08$, $g_2 = 2.00$, $g_3 = 1.95$) that had been evacuated at 573 K and then exposed to 20 Torr of water (8). Species D is assigned to Ru^{3+} coordinated to water molecules and zeolitic oxygen, $[Ru^{3+}(H_2O)_{n-m}(O_{zeo})_m^{-k}]^{3-k}$ (8). An EPR signal with parameters similar to those of species E has not been previously reported. Species E is still present after pretreatment at 573 and 673 K. Therefore, species E is assigned to $[Ru^{3+}(O_{zeo})_m^{-k}]^{3-k}$, a zeolite-bound ruthenium complex. It is possible that species E has one or more hydroxyl or water ligands. After pretreatment at 473 K, no signals remain that can be attributed to ruthenium–amine complexes, suggesting that the amine ligands are completely decomposed at this temperature.

The EPR spectrum acquired after the sample was heated to 573 K (Fig. 1D) is complex due to the presence of several overlapping signals. The EPR signals due to species C, D, and E are still present, although strong overlap with a new signal in the $g = 2.00$ region is evident. The new feature at $g = 2.20$ has been assigned as species F with EPR parameters: $g_1 = 2.20$, $g_2 = 2.02$, $g_3 = 1.87$. The g values of species F are similar to those previously assigned to lattice-bound Ru^{3+} in Ru–HX ($g_1 = 2.17$, $g_2 = 2.08$, $g_3 = 1.94$) (8). Analogously, species F is assigned to $[Ru^{3+}(O_{zeo})_m^{-k}]^{3-k}$. After the samples were heated to 673 K, the signals due to species C and D are not observed. The similarity in g values and the subsequent loss of both signals after heating of the samples to higher temperatures suggest that species C and D, $[Ru(H_2O)_5OH]^{2+}$ and $[Ru^{3+}(H_2O)_n(O_{zeo})_m^{-k}]^{3-k}$, respectively, have lost some or all of their water ligands to form species E and F.

The EPR spectrum acquired after heating Ru–Beta to 673 K exhibits signals assigned to species E and F. Species E and F are assigned to Ru^{3+} bound to oxygen of the zeolite framework, $[Ru^{3+}(O_{zeo})_m^{-k}]^{3-k}$. The EPR parameters for these two species are quite different, and this may reflect a different coordination environment for species E and F. For example, species E could have square planar coordination and species F could have square pyramidal coordination. Alternatively, species E could have different ligands than species F, resulting in different EPR parameters. For example, the EPR parameters for $Ru(H_2O)_6$ vs $Ru(NH_3)_6$ are very different (9, 13). In related work, the EPR parameters for Cu^{2+} species in copper-exchanged zeolites were sensitive to the geometry and the identity of the ligands (14–20).

The overall EPR signal intensity decreased by ~50% during the pretreatment process. One explanation is that part of the ruthenium EPR signal is lost because the ruthenium is converted into EPR silent species. Another possible explanation is that the spin-lattice relaxation times of the different ruthenium species vary, making the integration and calibration of the absolute number of spins difficult.

EPR Spectra of Ru–Y

The color of freshly exchanged Ru–Y was white and the color changed to wine-red after exposure to the atmosphere for an extended period of time (several weeks). This wine-red color is due to the formation of the trinuclear "Ru–red" complex, $[(NH_3)_5Ru^{III}ORu^{IV}(NH_3)_4ORu^{III}(NH_3)_5]^{6+}$, from reactions with air (21, 22). Care was taken to record EPR spectra prior to the formation of Ru–red complexes. The color of the fresh sample changed after pretreatment at 673 K to a dark gray color. Heating the sample to 373 K in the open atmosphere generated the same color.

Treatment of Ru–Y samples resulted in EPR spectra (Fig. 2) qualitatively similar to those obtained for Ru–Beta. Fresh Ru–Y yields an EPR spectrum acquired at 120 K with a broad, axial signal (species A*), with EPR parameters $g_\perp = 2.00$ and $g_\parallel = 1.73$. This ruthenium species has been designated as A* because it is analogous to species A in Ru–Beta; however, the EPR parameters are slightly different. This labeling scheme will be used throughout this paper. No EPR signal is observed at room temperature, indicating a short relaxation time for the ruthenium species (*vida supra*). This signal has been previously attributed to $[Ru(NH_3)_6]^{3+}$ exchanged into Na–Y (9).

EPR spectra recorded after heating Ru–Y to 373 and 473 K results in similar EPR spectra as shown in Fig. 1B, C. The EPR signal due to $[Ru(NH_3)_6]^{3+}$ is replaced with a rhombic EPR signal (species B*: $g_1 = 2.59$, $g_2 = 2.22$, $g_3 = 1.75$). A species with similar EPR parameters has previously been observed and attributed to $[Ru(NH_3)_5OH]^{2+}$ produced from reactions of $[Ru(NH_3)_6]^{3+}$ with adsorbed water in the zeolite channels (8, 9).

The EPR spectrum obtained after the sample was heated to 473 K (Fig. 2C) suggests that complete deammination of the ruthenium(III) complex in zeolite Y has occurred. The EPR spectrum is very complex and consists of several overlapping signals. The EPR spectrum is dominated by a signal (species D*) with EPR parameters $g_\perp = 2.07$ and $g_\parallel = 2.00$. Species D* is similar to that reported previously for Ru^{3+} bound to water and zeolitic oxygen, $[Ru^{3+}(H_2O)_n(O_{zeo})_m^{-k}]^{3-k}$ (8). This signal was presumed to be generated from the deammination of the $[Ru(NH_3)_5OH]^{2+}$ and the subsequent filling of the coordination sphere of Ru^{3+} by the adsorbed water in the zeolite. The probable location of this species is in the alpha cage, which has a free volume large enough to accommodate the aquoruthenium complex. Another signal (species C*) is present that overlaps the dominant signal and possesses

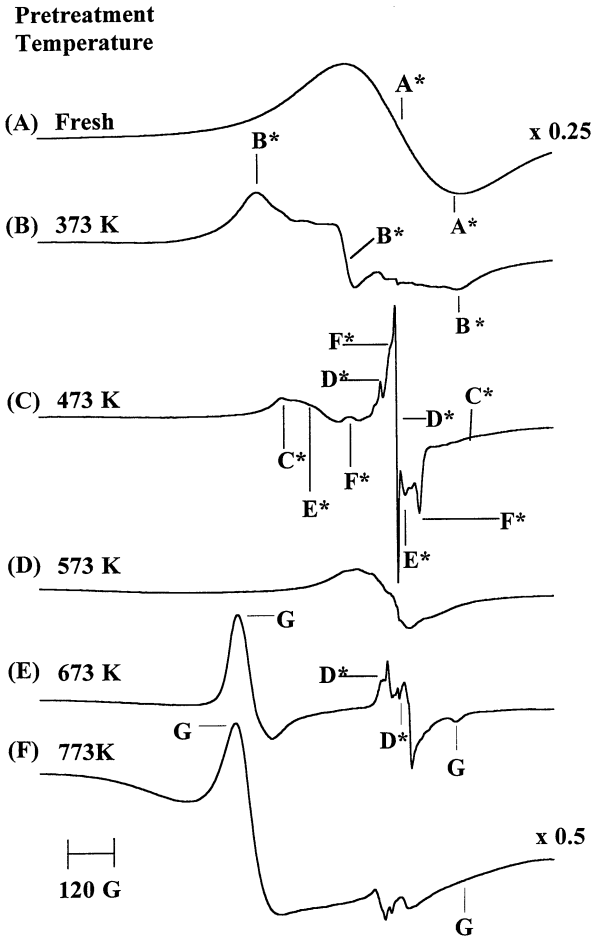

FIG. 2. EPR spectra of Ru–Y following pretreatment in helium at the indicated temperatures. EPR spectra were acquired at 120 K after sequential heating for 30 min: (A) fresh, (B) 373 K, (C) 473 K, (D) 573 K, and (E) 673 K. A fresh sample of Ru–Y was pretreated in helium at 773 K for several hours. The EPR spectrum of Ru–Y pretreated at 773 K and recorded at 120 K is shown in (F).

a component in the low-field and high-field regions ($g_\perp = 2.47$, $g_\parallel = 1.75$). The weaker signal (species C*) present in the EPR spectrum is attributed to $[Ru(H_2O)_5OH]^{2+}$ in Ru–Y (13). These ruthenium species are analogous to species C and D in Ru–Beta and they have been labeled as C* and D* to distinguish them from species C and D in Ru–Beta because the EPR parameters are slightly different. The differences in EPR parameters can be attributed to differences in the local environments or sites of the ruthenium species in the different zeolites.

Two overlapping, axial signals in the high-field region (species E* and F*) are also observed in Fig. 2C. The two overlapping, axial signals are assigned as species E* with $g_\perp = 1.94$ and $g_\parallel = 2.41$ and species F* with $g_1 = 2.21$, $g_2 = 2.03$, and $g_3 = 1.90$. These species are assigned to zeolite-bound $[Ru^{3+}(O_{zeo})_m^{-k}]^{3-k}$ complexes with different coordination environments. The EPR assignments are summarized in Table 3.

After the sample was heated to 573 K, the EPR spectrum of Ru–Y is rather broad and featureless. A new feature emerges after heating Ru–Y to 673 K in helium. This is assigned as species G and has $g_\perp = 2.69$ and $g_\parallel = 1.76$. This spectral feature assigned to species G is also very prominent in the spectrum of a separate sample of Ru–Y that had been heated in helium at 773 K for several hours (outside of the EPR spectrometer) and is shown in Fig. 2F. Since species G is already present after pretreatment in helium at elevated temperatures, it is assigned to a Ru^{3+} complex bound to oxygen of the zeolite lattice, analogous to species E and F. However, the EPR parameters of species G are quite different from those of the other zeolite-bound ruthenium species observed in this and other work as can be seen from inspection of Tables 2 and 3. The g anisotropy is very large and the signal is similar in this regard to that of the original $[Ru(NH_3)_6]^{3+}$ or $[Ru(NH_3)_5OH]^{2+}$ complexes. However, there should not be any additional ligands present, so the change in EPR signal is attributed to a change in the crystal field of the Ru^{3+} ion.

The EPR spectral intensity decreases by ~85% during the course of helium pretreatment to 673 K. The signal intensity of the EPR spectrum (Fig. 2F) obtained for the Ru–Y sample pretreated at 773 K will not be compared with the signal intensities in Fig. 2A–E since a fresh Ru–Y sample was used for the helium pretreatment at 773 K.

EPR Spectra of Ru–ZSM-5

The freshly exchanged Ru–ZSM-5 sample was white in color. The sample was brown after pretreatment in helium at elevated temperatures, and after subsequent exposure to the atmosphere for several days, the sample color changed to a greenish gray.

The EPR spectra acquired during the pretreatment of Ru–ZSM-5 are shown in Fig. 3. The EPR spectra of fresh Ru–ZSM-5 and Ru–ZSM-5 pretreated at 373 K exhibit several low-intensity signals. The characteristic EPR signal for $[Ru(NH_3)_6]^{3+}$ observed in Ru–Beta and Ru–Y was not observed. The lack of the $[Ru(NH_3)_6]^{3+}$ EPR signal suggests that either this species is not present in Ru–ZSM-5 or that the spin-lattice relaxation time of the ruthenium complex is very short and would require cooling to 4 K.

After the sample was heated to 473 K, several overlapping signals appear in the EPR spectrum, Fig. 3C. Due to the low intensity and complexity of this EPR spectrum, the individual components of the EPR spectrum were not assigned. Heating the sample to 573 K produces a much more intense EPR signal, relative to the fresh sample. The main component of the signal is labeled species D** with g values of $g_1 = 2.06$ and $g_2 = 2.01$. This species has g values that are similar to species D and D* in Ru–Beta and Ru–Y and is similarly assigned $[Ru^{3+}(H_2O)_n(O_{zeo})_m^{-k}]^{3-k}$. A second relatively weak signal is assigned as species E** ($g_1 = 1.95$ and $g_2 = 2.41$) by comparison with the EPR spectra for

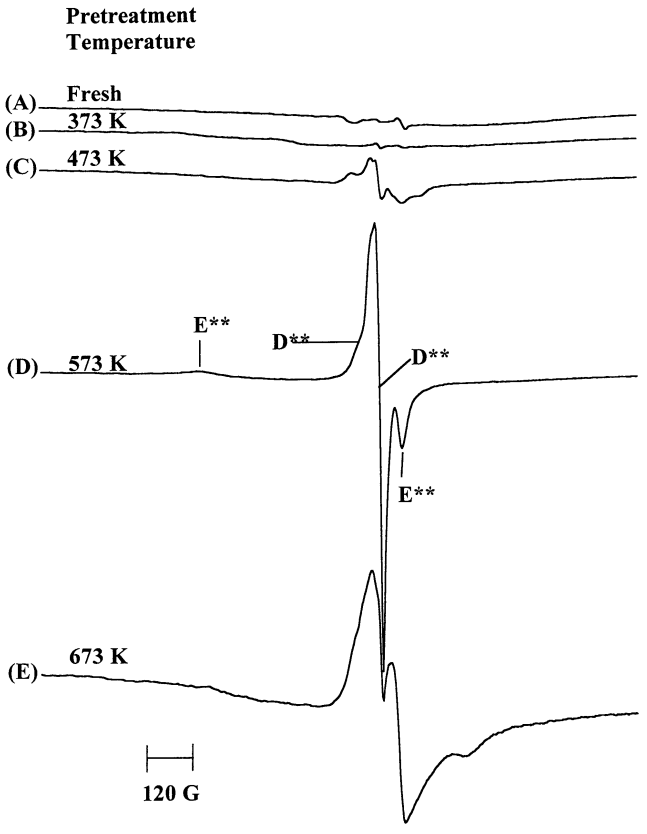

FIG. 3. EPR spectra of Ru–ZSM-5 following pretreatment in helium at the indicated temperatures. EPR spectra were acquired at 120 K after sequential heating for 30 min: (A) fresh, (B) 373 K, (C) 473 K, (D) 573 K, and (E) 673 K.

Ru–Beta and Ru–Y. Species E^{**} is assigned as a zeolite-bound species, $[Ru^{3+}(O_{zeo})_m^{-k}]^{3-k}$.

Heating the sample to 673 K results in a broadened EPR spectrum (Fig. 3E) relative to the spectrum obtained after pretreatment at 573 K. Presumably, this is due to the presence of several overlapping signals in the EPR spectrum. The features of the spectra indicate at least two overlapping signals that correspond to D^{**} and E^{**} from the previous spectrum in Fig. 3D. A third species has a g_2 or g_3 value of 1.80 with the other features unresolved due to spectral overlap and broadening.

EPR after N_2O Decomposition on Ru–Y at Different Temperatures

The EPR spectra obtained after exposure of Ru–Y to N_2O in helium at various temperatures are shown in Fig. 4. The Ru–Y sample used was not pretreated prior to this experiment. A fresh Ru–Y sample was heated to 373 K and held there for 30 min, followed by exposure to 3300 ppm N_2O in helium for 15 min. The catalytic activity of the EPR sample was measured by GC and then the sample was purged with helium for 10 min at 373 K and cooled to 120 K in helium flow for EPR data acquisition. This procedure was repeated at consecutively higher temperatures, 473, 573, and 673 K. At each temperature, the N_2O conversion to N_2 was measured by GC and an EPR spectrum was obtained after cooling of the sample.

The EPR spectrum obtained after exposure to N_2O in helium at each of the temperatures is shown in Fig. 4A–D, respectively. The conversion of N_2O to N_2 measured by GC at each temperature is shown on the right side of the figure. The EPR spectra obtained after treatment in N_2O at 373 and 473 K (Fig. 4A,B) are almost identical to those shown in Fig. 2B,C for the pretreatment in helium at comparable temperature. The EPR spectrum obtained after exposure to N_2O in helium at 573 K begins to show a new spectral feature at $g = 2.69$ that can be assigned to species G, analogous to the helium-treated case. This EPR signal first appears after pretreatment at 573 K and increases after exposure to N_2O in helium at 673 K. Correspondingly, the catalytic activity increases from 10 to 49% as the EPR feature assigned to species G increases in size.

Similar experiments were conducted on Ru–Beta and Ru–ZSM-5, but an analogous correlation of the EPR signal with N_2O activity was not observed. The EPR spectra

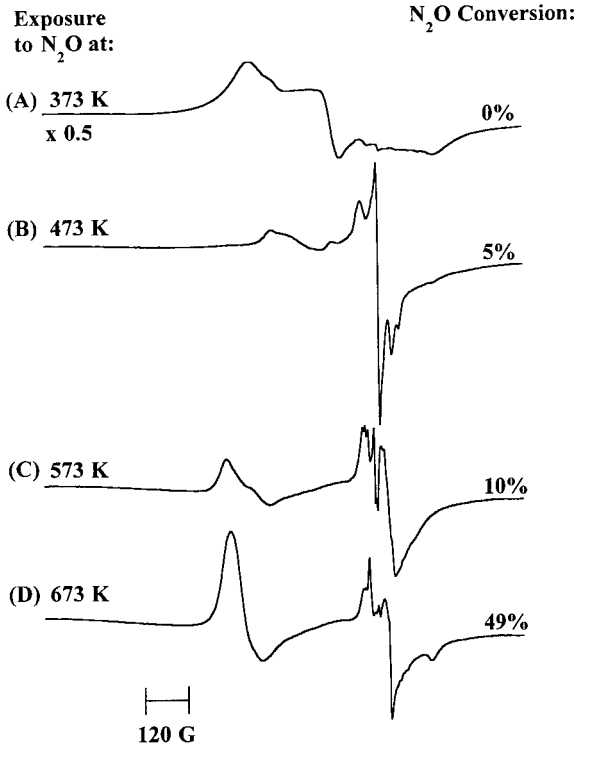

FIG. 4. EPR spectra acquired at 120 K after exposure of Ru–Y to N_2O at various temperatures. Ru–Y was heated in helium to the temperature and then was exposed to N_2O (3333 ppm N_2O in helium) for 15 min at the indicated temperatures: (A) 373 K, (B) 473 K, (C) 573 K, and (D) 673 K. N_2O conversion to N_2 was measured by GC and the conversions are indicated in the figure. After the GC activity measurement, the sample was cooled to 120 K for EPR data acquisition.

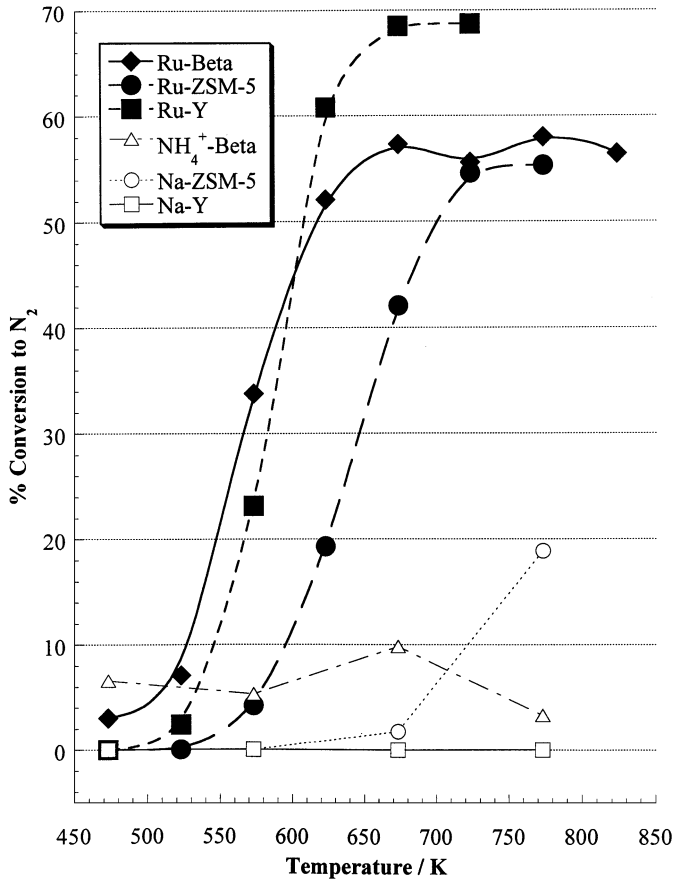

FIG. 5. Catalytic decomposition of nitrous oxide over Ru–Beta (▲), Ru–Y (■), Ru–ZSM-5 (●), NH_4^+–Beta (△), Na–Y (□), and NaZSM-5 (○) Samples were pretreated for 1 h at 773 K in helium prior to activity measurements.

acquired before and after exposure to N_2O were almost identical.

Catalytic Activity Measurements

Figure 5 shows the percent conversion of nitrous oxide to nitrogen as a function of temperature for each of the ruthenium-exchanged zeolites and the parent zeolites after pretreatment at 773 K in helium. Ru–Y exhibited the highest activity (68% at 673 K), while Ru–ZSM-5 and Ru–Beta reached similar activities (55%) at 723 and 673 K, respectively. None of the parent zeolites, NH_4^+–Beta, Na–Y, or Na–ZSM-5, exhibited appreciable activity for N_2O decomposition under comparable experimental conditions. In particular, NH_4^+–Beta (which is almost certainly H–Beta after pretreatment) showed a conversion of <10% at the temperatures tested.

All three catalysts exhibited activity for the direct decomposition of N_2O with the order of maximum conversion given by Ru–Y > Ru–Beta > Ru–ZSM-5 (Fig. 5). The maximum conversion for Ru–ZSM-5 (~55% at 698 K) was lower than that obtained by Li and Armor (3) (~100% at 623 K). This difference may be due to the lower Ru loading used in this study, 0.2wt% in this work and 0.6 wt% in Li and Armor.

IV. DISCUSSION

Comparison of EPR Spectra of Ru–Beta, Ru–Y, and Ru–ZSM-5

Ru^{3+} species with qualitatively similar EPR signals were observed in fresh Ru–Beta and fresh Ru–Y samples. Initially, a broad EPR signal attributed to $[Ru(NH_3)_6]^{3+}$ (species A and A*) was observed in Ru–Beta and Ru–Y. After Ru–Beta and Ru–Y were heated to 373 K in helium, $[Ru(NH_3)_6]^{3+}$ decomposed according to reaction [2]. The loss of the amine ligand leaves a vacancy in the coordination sphere of the ruthenium cation, and a hydroxyl molecule formed from adsorbed water fills this vacancy. EPR signals observed after pretreatment of Ru–Beta and Ru–Y at 373 K were attributed to the hydroxyl complex, $[Ru(NH_3)_5OH]^{2+}$ (species B and B*). As indicated by a comparison of the data in Tables 2 and 3, similar EPR signals for $[Ru(NH_3)_6]^{3+}$ and $[Ru(NH_3)_5OH]^{2+}$ in zeolites have been reported in previous studies of ruthenium-exchanged X and Y (7–9).

After pretreatment at 473 K, Ru–Beta and Ru–Y exhibited EPR signals that were attributed to completely deamminated ruthenium complexes. Adsorbed water can react with the amine ligands to generate the deamminated complexes according to reactions [3] and [4]. These water complexes were observed to decompose after heating at higher temperatures. Sheu and co-workers reported that all of the amine ligands in ruthenium-exchanged Y were removed after heating to 673 K (23). EPR results in this paper suggest that the amine ligands are removed between 373 and 473 K under these experimental conditions. A number of groups have reported that ruthenium nitrosyl species, such as $[Ru(NH_3)_4(NO)OH]^{2+}$ or $[Ru(NH_3)_4(NO)H_2O]^{3+}$, are formed during pretreatment of Ru–Y at elevated temperatures (23–25). Spin pairing of the unpaired electron spins of Ru^{3+} and NO would result in a loss of EPR signal. A loss of EPR signal was observed in this study during pretreatment of Ru–Y and Ru–Beta; this is consistent with the formation of ruthenium nitrosyl species but there are a number of other possibilities as well. The paramagnetic ruthenium species observed after pretreatment at 473 K were assigned to Ru^{3+} bound to the zeolite lattice with or without water molecules filling the vacant coordination sites and to Ru^{3+} with water and hydroxyl molecules filling the coordination sphere with no binding to the zeolite lattice. After pretreatment of Ru–Beta and Ru–Y at 673 K, many of the same species are observed in the EPR spectra as were observed in the EPR spectra at 473 and 573 K, but the relative intensities have changed. A new species G is observed in the EPR spectrum of Ru–Y after pretreatment at 673 or 773 K in helium.

EPR spectra of Ru–ZSM-5 during pretreatment exhibited different spectral characteristics when compared to the EPR spectra of Ru–Beta and Ru–Y. Initially, the EPR spectrum of the freshly exchanged Ru–ZSM-5 sample is very weak. An EPR signal from $[Ru(NH_3)_6]^{3+}$ was not observed. This could be due to relaxation effects as discussed earlier in this paper or it is possible that the $[Ru(NH_3)_6]^{3+}$ complex is too large to fit in the pores of ZSM-5. After pretreatment in helium at various temperatures, the EPR spectra of the Ru-exchanged zeolites contained some of the same signals, as can be seen by inspection of Table 3.

Overall, the EPR spectra of Ru-exchanged zeolites after various pretreatments suggested the presence of some similar ruthenium species in all samples, regardless of the parent zeolite. However, differences in the specific EPR parameters and the relative intensities of different spectral features were apparent, depending on the identity of the parent zeolite. In particular, the EPR spectra of the Ru–ZSM-5 sample used in this study were quite different from the EPR spectra of Ru–Beta and Ru–Y.

Implications for Catalytic Activity

All of the Ru-exchanged zeolite samples used in this study exhibited substantial catalytic activity for N_2O decomposition. Chang and co-workers previously suggested that ionic Ru^{3+} was responsible for the N_2O decomposition activity in Ru–Y (4). In this study, direct EPR observation of Ru^{3+} species are reported in Ru–Beta, Ru–Y, and Ru–ZSM-5 samples that are active for N_2O decomposition. However, it is difficult to prove that the Ru^{3+} species that are observed in the EPR spectra are the species responsible for the N_2O decomposition activity. The relative EPR signal intensity decreases as fresh samples of Ru–Beta and Ru–Y are pretreated at elevated temperatures. The decrease in signal intensity indicates that a substantial portion of the ruthenium in pretreated samples is EPR silent. Therefore, any conclusions that are made relating the catalytic activity to the observed EPR signals must be qualified by this realization that all of the ruthenium is not observed in the EPR spectra.

From a catalytic perspective, perhaps the most intriguing results are those presented in Fig. 4 in which EPR spectra were acquired after Ru–Y was exposed to N_2O under realistic decomposition conditions. Since the EPR signals for Ru-exchanged zeolites could not be observed at elevated temperatures, the conversion of N_2O to N_2 was measured prior to cooling the Ru–Y sample for EPR data acquisition. Due to the cooling of the sample, it is unlikely that any intermediate species would be observed in the EPR spectra. However, the data clearly show that as the EPR signal assigned to species G increases, the conversion of N_2O to N_2 also increases. A similar species was not observed in the EPR spectra of Ru–Beta and Ru–ZSM-5. This correlation of an EPR signal with catalytic activity suggests that this species might be important in the decomposition of N_2O to N_2 on Ru–Y. However, further studies need to be done to investigate this correlation of EPR signal and catalytic activity and to more definitively identify species G.

V. CONCLUSIONS

EPR spectroscopy was used to characterize a series of ruthenium-exchanged zeolites, Ru–Y, Ru–Beta, and Ru–ZSM-5. Ruthenium was exchanged into the zeolites as $[Ru(NH_3)_6]^{3+}$. The EPR signal observed for fresh Ru–Beta and Ru–Y was assigned to the intact $[Ru(NH_3)_6]^{3+}$ complex. A similar signal was not observed for Ru–ZSM-5. After pretreatment at 373, 473, 573, and 673 K, respectively, complex EPR spectra were obtained that contained overlapping signals. When spectral simulation and spectral subtraction were used, many of the EPR features were assigned to various Ru^{3+} species containing water and hydroxyl ligands. Some similar overlapping EPR signals were observed in the different zeolites, but the relative intensities of the signals varied. Catalytic activity measurements indicated that the ruthenium-exchanged zeolites used in this study were active for N_2O decomposition. A specific EPR signal in Ru–Y was correlated with the onset of catalytic activity.

ACKNOWLEDGMENTS

S.L. gratefully acknowledges the support of NSF (CTS-99-73431) and the University of Iowa. The authors would also like to thank Susan Dorholt for catalytic activity measurements.

REFERENCES

1. Verdonck, J. J., Jacobs, P. A., and Uytterhoeven, J. B., *J. Chem. Soc. Chem. Commun.* 181 (1979).
2. Jacobs, P. A., Nijsand, N. H., and Uytterhoeven, J. B., *Prepr.-Am. Chem. Soc. Div. Pet. Chem.* **23**, 469 (1978).
3. Li, Y., and Armor, J. N., *Appl. Catal. B: Environ.* **1**, L21–L29 (1992).
4. Chang, Y.-F., McCarty, J. G., and Wachsman, E. D., *Appl. Catal. B: Environ.* **6**, 21–33 (1995).
5. Chang, Y.-F., McCarty, J. G., Wachsman, E. D., and Wong, V. L., *Appl. Catal. B: Environ.* **4**, 283–299 (1994).
6. Gustafson, B. L., Lin, M.-J., and Lunsford, J. H., *J. Phys. Chem.* **84**, 3211–3215 (1980).
7. Lei, G.-D., and Kevan, L., *J. Phys. Chem.* **94**, 6384–6390 (1990).
8. Lei, G.-D., and Kevan, L., *J. Phys. Chem.* **95**, 4506–4514 (1991).
9. Goldwasser, M., Dutel, J. F., and Naccache, C., *Zeolites* **9**, 54–58 (1989).
10. Rollmann, L. D., and Valyocsik, E. W., *in* "Inorganic Syntheses" (Holt, S. L., Ed.), p. 61, Vol. 22. Wiley Interscience, New York, 1983.
11. Carl, P. J., and Larsen, S. C., *J. Catal.* **182**, 208–218 (1999).
12. Bunker, B. C., Drago, R. S., Hendrickson, D. N., Richman, R. M., and Kessell, S. L., *J. Am. Chem. Soc.* **100**, 3805–3814 (1978).
13. Wan, B.-Z., and Lunsford, J. H., *Inorg. Chim. Acta.* **65**, L29–L30 (1982).
14. Attfield, M. P., Weigel, S. J., and Cheetham, A. K., *J. Catal.* **170**, 227–235 (1997).
15. Anderson, M. W., and Kevan, L., *J. Phys. Chem.* **91**, 4174–4179 (1987).

16. Larsen, S. C., Aylor, A., Bell, A. T., and Reimer, J. A., *J. Phys. Chem.* **98**, 11533–11539 (1994).
17. Kucherov, A. V., Slinkin, A. A., Kondrat'ev, D. A., Bondaranko, T. N., Rubinshtein, A. M., and Minachev, K. M., *Kinet. Katal.* **26**, 409–415 (1985).
18. Schoonheydt, R. A., *Catal. Rev.-Sci. Eng.* **35**, 129–168 (1993).
19. Oliva, C., Selli, E., Ponti, A., Correale, L., Solinas, V., Rombi, E., Monaci, R., and Forni, L., *J. Chem. Soc. Faraday Trans.* **93**, 2603–2608 (1997).
20. Smith, D. W., *J. Chem. Soc. A* 3108–3120 (1970).
21. Madhusudhan, C. P., Patil, M. D., and Good, M. L., *Inorg. Chem.* **18**, 2384–2389 (1979).
22. Fletcher, J. M., Greenfield, B. F., Hardy, C. J., Scargill, D., and Woodhead, J. L., *J. Chem. Soc.* **1961**, 2000–2006 (1961).
23. Sheu, S.-P., Karge, H. G., and Schlogl, R., *J. Catal.* **168**, 278–291 (1997).
24. Verdonck, J. J., Shoonheydt, R. A., and Jacobs, P. A., *J. Phys. Chem.* **85**, 2393–2398 (1981).
25. Pearce, J. R., Gustafson, B. L., and Lunsford, J. H., *Inorg. Chem* **20**, 2957–2960 (1981).